**Supporting Information**

# From Toxic Pollutant to Catalyst: One-Pot Synthesis of $Fe_3O_4$-Ni-DBP/NF for Efficient Overall Water Splitting

Qingyuan Song [a, b], Jinshou Yao [a], Liujun Jin [a, *], Peiyang Gu [a], Ye Wang [c], Ping Liu [a, *], Congping Chen [c], Guohong Dai [c, d*]

[a] *School of Petrochemical Engineering, Changzhou University, Changzhou, 213164, PR China*

[b] *School of Safety Science and Engineering, Changzhou University, Changzhou, 213164, Jiangsu, PR China*

[c] *School of Mechanical Engineering and Rail Transit, Changzhou University, Changzhou, 213164, Jiangsu, PR China*

[d] *School of Mechanical Engineering, Jiangsu University of Technology, Changzhou, 213164, Jiangsu, PR China*

*E-mail: jinlj@cczu.edu.cn, pingliu@cczu.edu.cn, dgh@cczu.edu.cn*

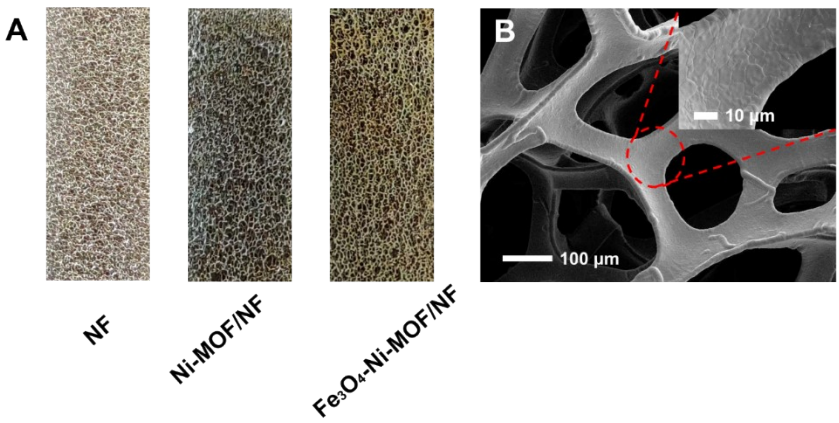

**Figure S1.** (A) Color changes in the appearance of the NF, Ni-DBP, and $Fe_3O_4$-Ni-DBP. (B) FE-SEM image of bare NF.

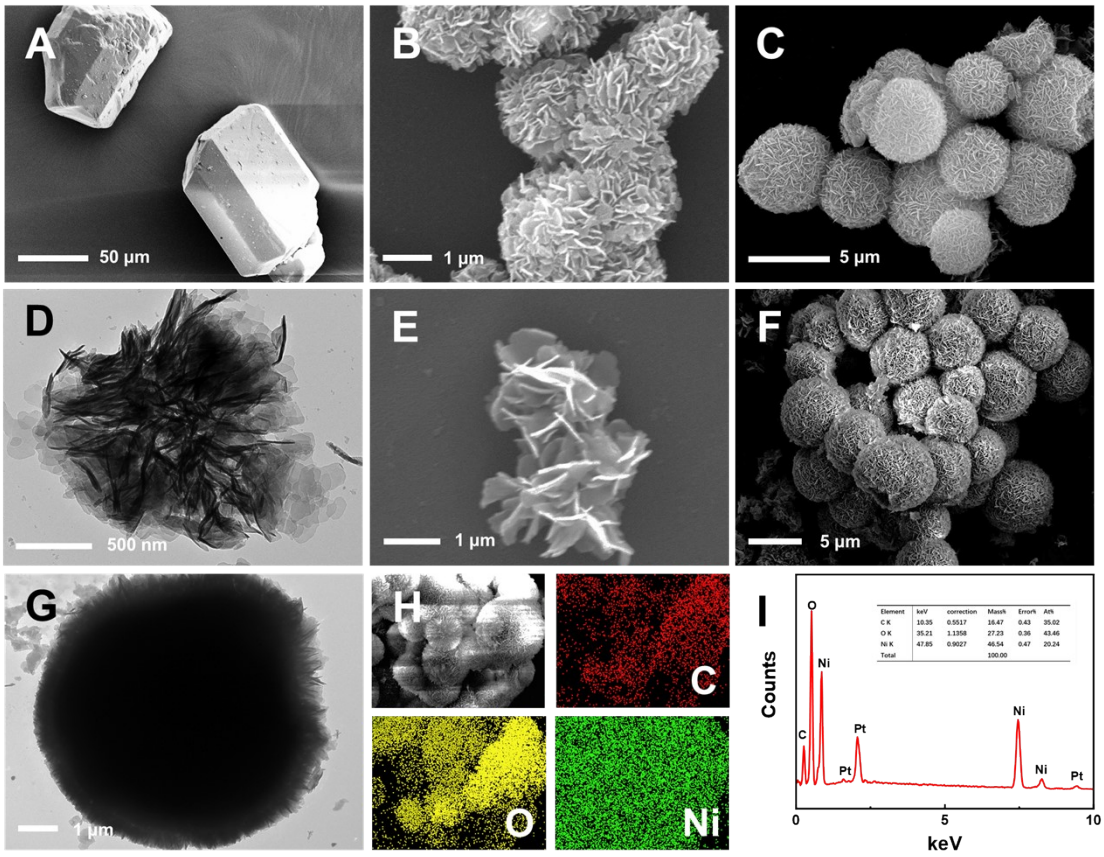


**Figure S2.** FE-SEM morphologies of (A) 1,2-BDC, (B) Ni-BDC (without PVP), (C) Ni-BDC. (D) TEM morphology of Ni-BDC. SEM morphologies of (E) Ni-DBP (without PVP), (F) Ni-DBP. (G) TEM morphology of Ni-DBP. (H) Elemental mapping analyses of the Ni-DBP. (I) EDS spectrogram of the Ni-DBP.

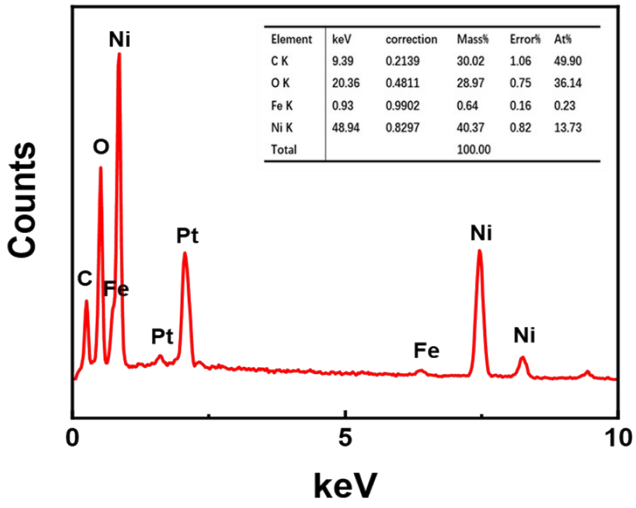


**Figure S3.** EDS spectrogram of the $Fe_3O_4$-Ni-DBP/NF.

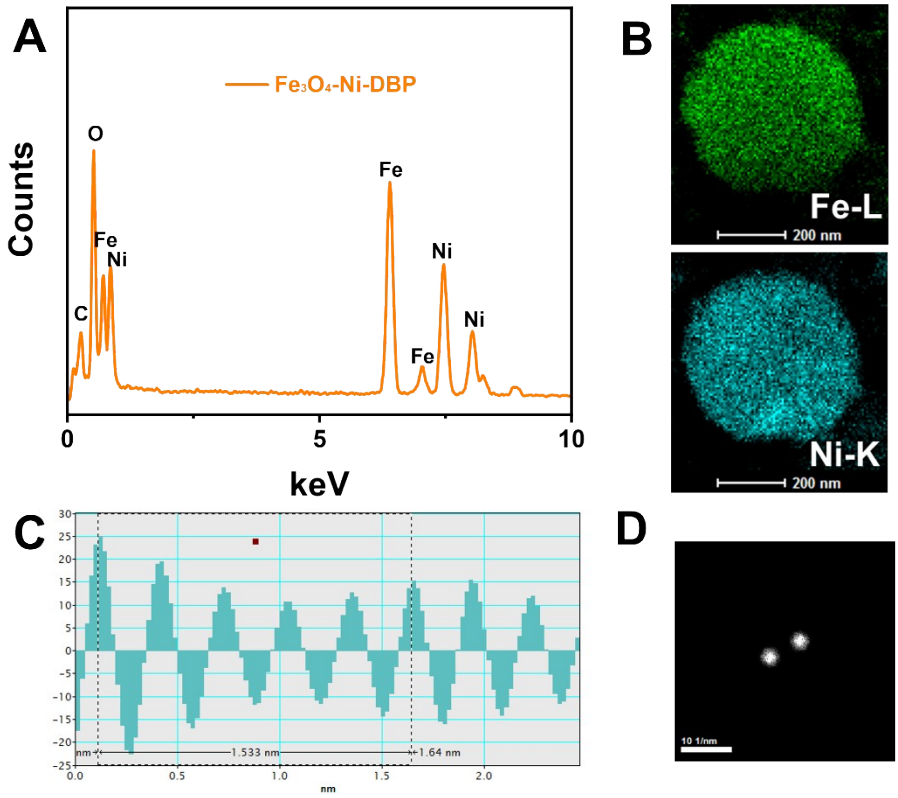


**Figure S4.** (A) TEM-EDS spectrogram of the $Fe_3O_4$-Ni-DBP. (B) Elemental mapping analyses of the Fe-L and Ni-K for $Fe_3O_4$-Ni-DBP. (C) Height profile and (D) topographic image of the inverse FFT mode.

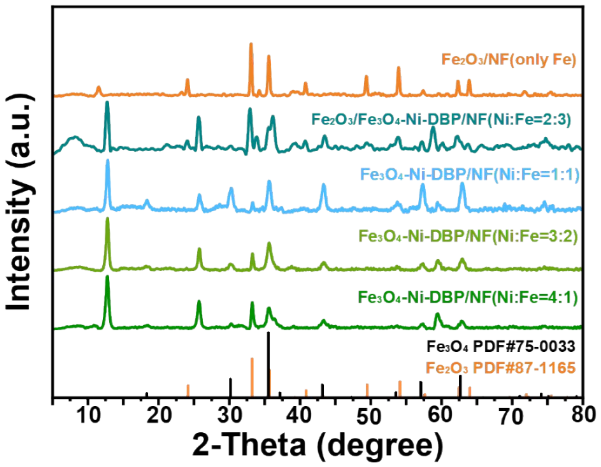


**Figure S5.** PXRD patterns of $Fe_3O_4$-Ni-DBP with different metal ratios.

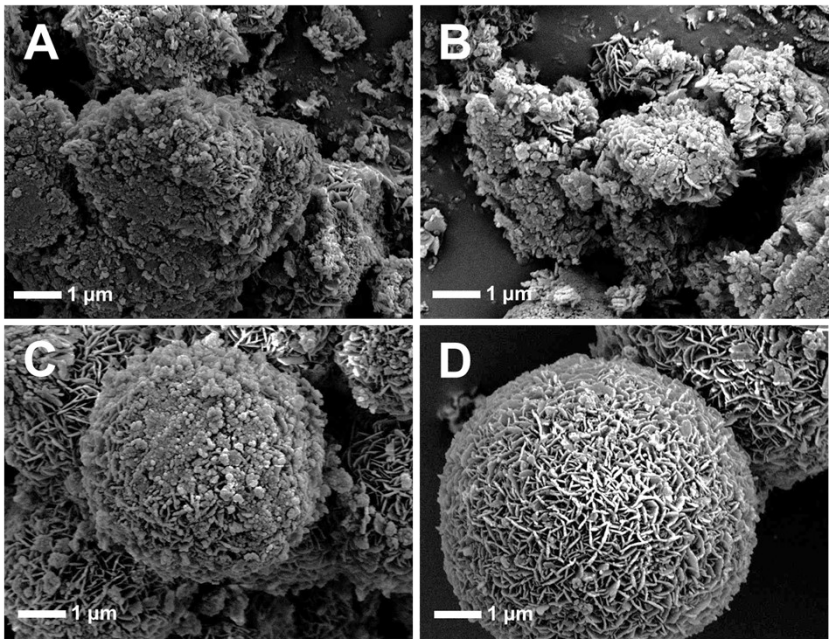


**Figure S6.** FE-SEM images of (A) $Fe_3O_4$-Ni-DBP with different metal ratios: (A) Ni:Fe = 1:4, (B) Ni:Fe = 2:3, (C) Ni:Fe = 3:2, and (D) Ni:Fe = 4:1.

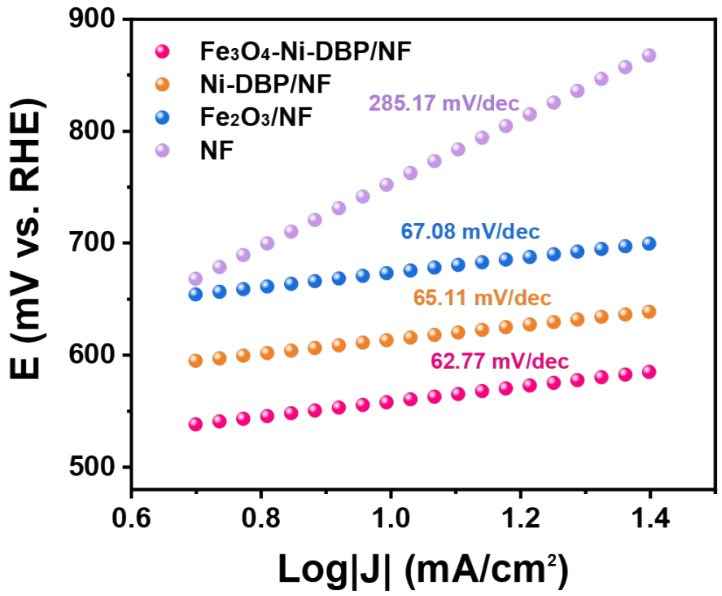


**Figure S7.** Tafel plot of $Fe_3O_4$-Ni-DBP/NF, Ni-DBP/NF, $Fe_2O_3$/NF, and bare NF for the OER derived from steady-state polarization measurements.

**Table S1.** OER performance of various electrocatalysts.

| Electrocatalysts | OER $\eta_{10}$ [a] (mV) | Tafel Slope (mV/dec) | Reference |
|---|---|---|---|
| Ni/FeOx NRs@CP | 242 | 80.40 | [1] |
| $WO_3$ NRs@Co-MOF/NF | 280 | 36.00 | [2] |
| Ni-MOF/NF-SS | 253 | 70.90 | [3] |
| $(Ni, Co)_2P$/NFs | 283 | 56.40 | [4] |
| $Ni_3Se_2$@NiFe-LDH/NF | 222 | 61.30 | [5] |
| Mo-$CoSe_2$NS@NF | 234 | 58.00 | [6] |
| $MoS_2/NiS_2/CoS_2$ | 230 | 89.00 | [7] |
| **$Fe_3O_4$-Ni-DBP/NF** | **233** | **55.34** | **This work** |

a: The overpotential (mV) required to drive a current density of 10 mA $cm^{-2}$ in 1.0 M KOH.

**Figure S8.** CV(OER) curves of the (A) $Fe_3O_4$-Ni-DBP/NF, (B) Ni-DBP/NF, (C) $Fe_2O_3$/NF with varying scan rates (10, 20, 30, 40, 50 mV/s) in 1.0 M KOH. (D) The $C_{dl}$ values of different catalysts.

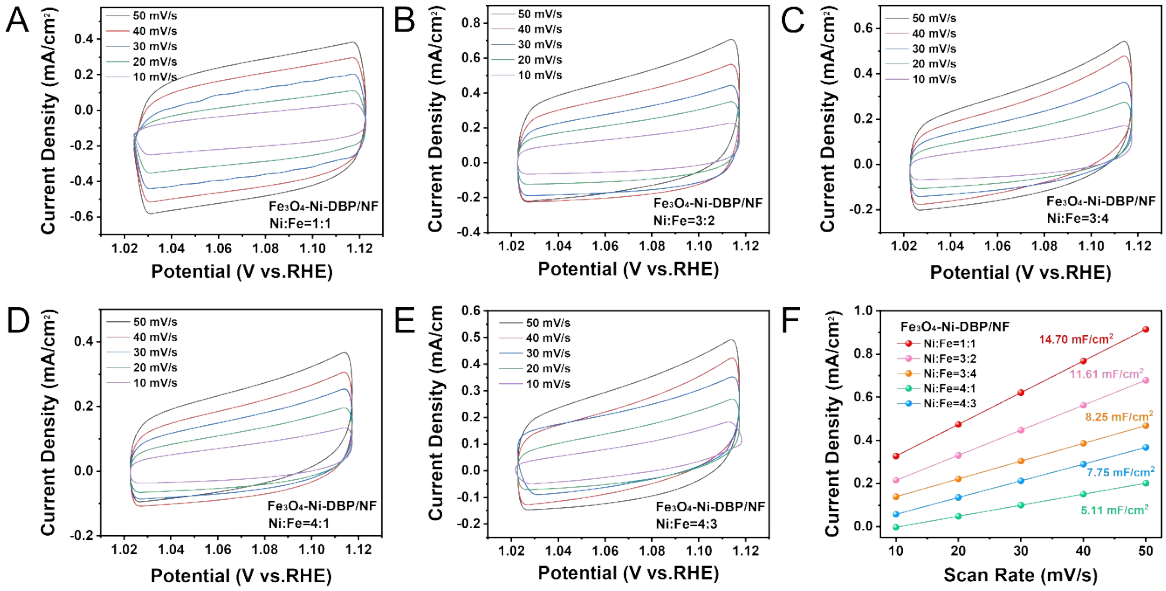


**Figure S9.** CV(OER) curves of the $Fe_3O_4$-Ni-DBP/NF with different metal ratios: (A) Ni:Fe = 1:1, (B) Ni:Fe = 3:2, (C) Ni:Fe = 3:4, (D) Ni:Fe = 4:1, (E) Ni:Fe = 4:3 with varying scan rates (10, 20, 30, 40, 50 mV/s) in 1.0 M KOH. (F) The $C_{dl}$ values of different metal ratios.

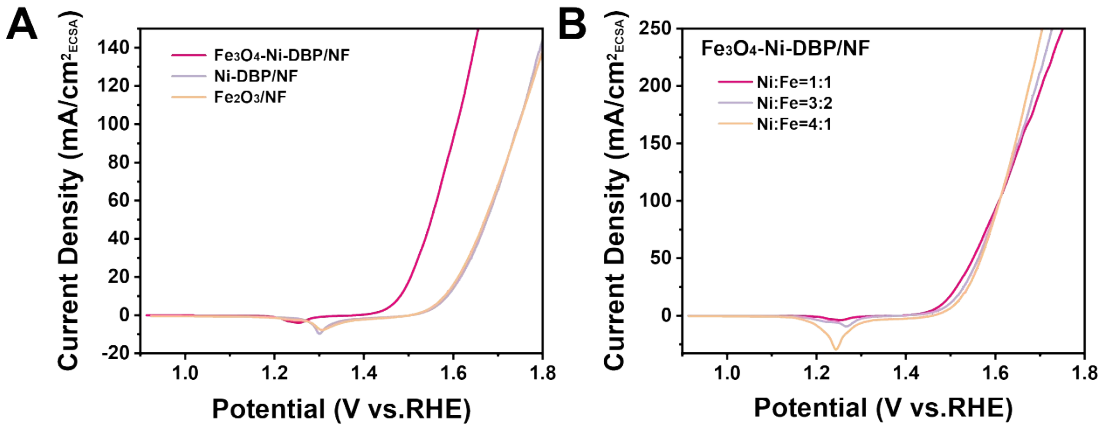


**Figure S10.** Normalized LSV curves based on ECSA (specific capacitance $C_S$ = 40 μF cm$^{-2}$): (A) different catalysts, (B) different metal ratios.

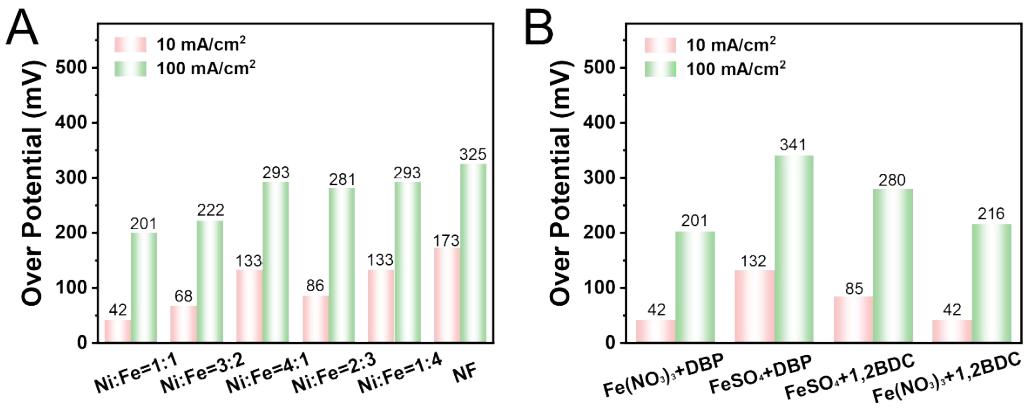


**Figure S11.** Overpotentials derived from HER polarization curves at 10 mA $cm^{-2}$ and 100 mA $cm^{-2}$: (A) $Fe_3O_4$-Ni-DBP/NF with different metal ratios, (B) $Fe_3O_4$-Ni-DBP/NF prepared by different alternative precursors.

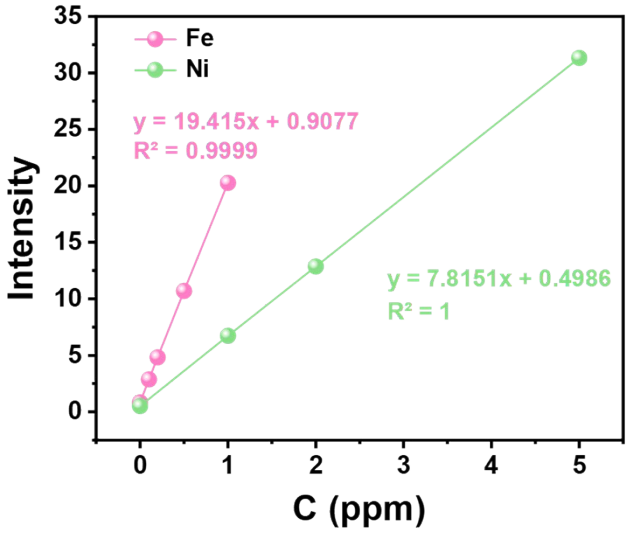


**Figure S12.** ICP-OES calibration curves of Fe and Ni ions.

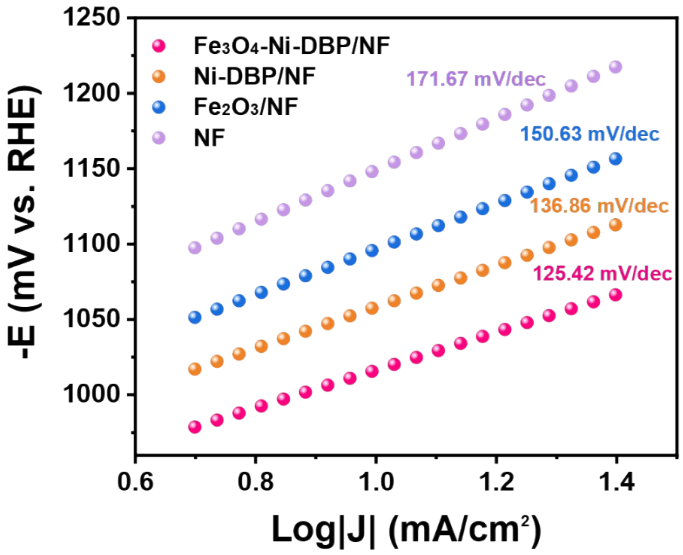


**Figure S13.** Tafel plot of $Fe_3O_4$-Ni-DBP/NF, Ni-DBP/NF, $Fe_2O_3$/NF, and bare NF for the HER derived from steady-state polarization measurements.

**Table S2.** HER performance of various electrocatalysts.

| Electrocatalysts | HER $\eta_{10}$ [a] (mV) | Tafel Slope (mV/dec) | Reference |
|---|---|---|---|
| Mn-MOF/NF | 125 | 113.00 | [8] |
| $(Ni, Co)_2P$ NFs | 92 | 62.30 | [4] |
| $Ni_3Se_2$@NiFe-LDH/NF | 68 | 106.20 | [5] |
| NiFe-LDH-POM/NF | 156 | 86.00 | [9] |
| Mo-$CoSe_2$NS@NF | 89 | 69.00 | [6] |
| $MoS_2/NiS_2/CoS_2$ | 101 | 116.00 | [7] |
| $Co_8FeS_8$MXene/NF | 108 | 84.08 | [10] |
| **$Fe_3O_4$-Ni-DBP/NF** | **42** | **39.16** | **This work** |

a: The overpotential (mV) required to drive a current density of 10 mA $cm^{-2}$ in a 1.0 M KOH.

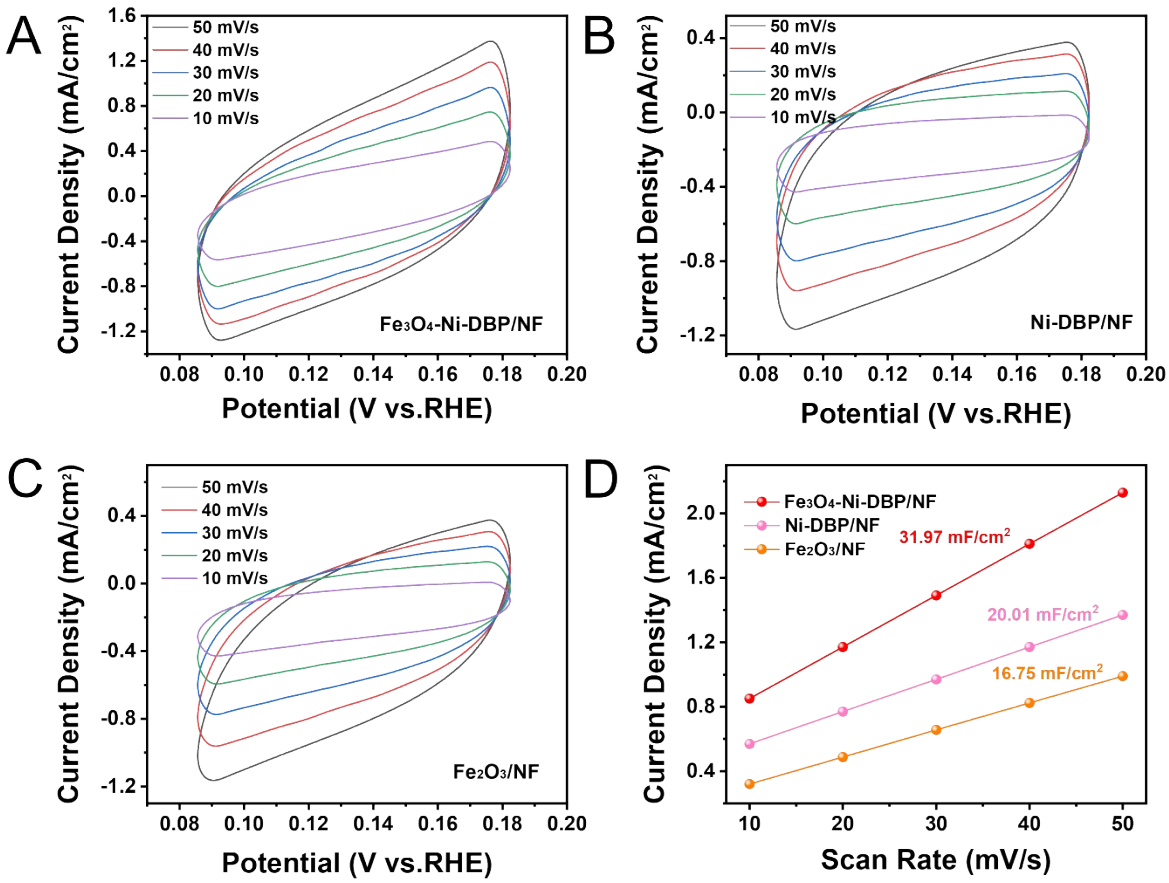


**Figure S14.** CV(HER) curves of the (A) $Fe_3O_4$-Ni-DBP/NF, (B) Ni-DBP/NF, (C) $Fe_2O_3$/NF with varying scan rates (10, 20, 30, 40, 50 mV/s) in 1.0 M KOH. (D) The $C_{dl}$ values of different catalysts.

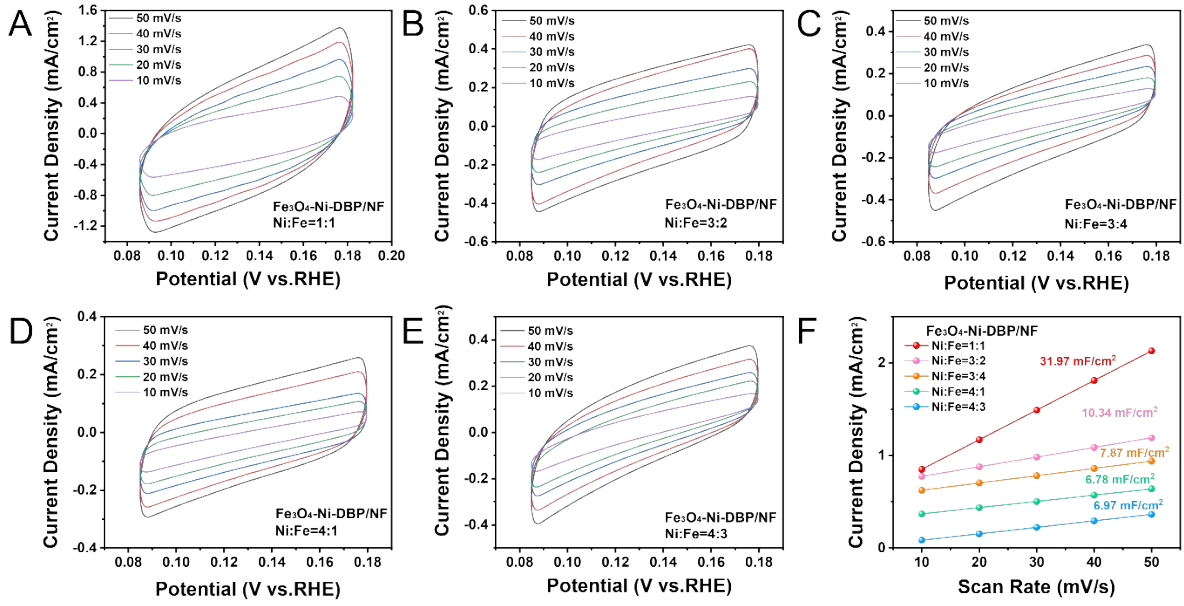


**Figure S15.** CV(HER) curves of the $Fe_3O_4$-Ni-DBP/NF with different metal ratios: (A) Ni:Fe = 1:1,

(B) Ni:Fe = 3:2, (C) Ni:Fe = 3:4, (D) Ni:Fe = 4:1, (E) Ni:Fe = 4:3 with varying scan rates (10, 20, 30, 40, 50 mV/s) in 1.0 M KOH. (F) The $C_{dl}$ values of different metal ratios.

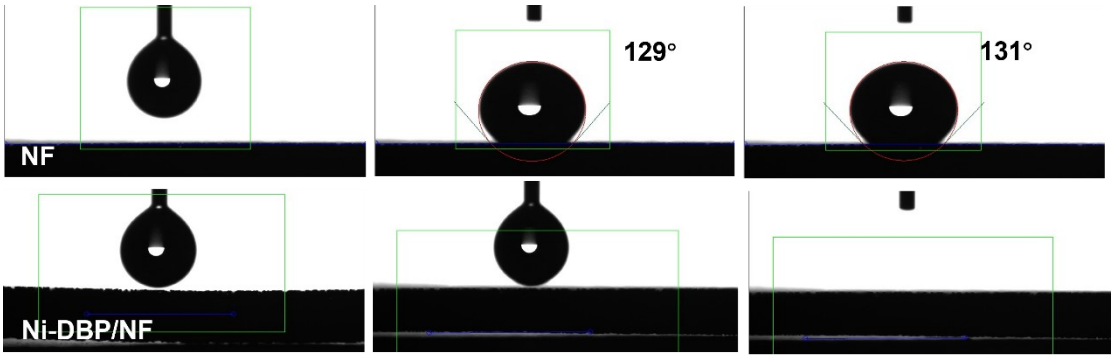


**Figure S16.** The static water contact angle of NF and Ni-DBP/NF.

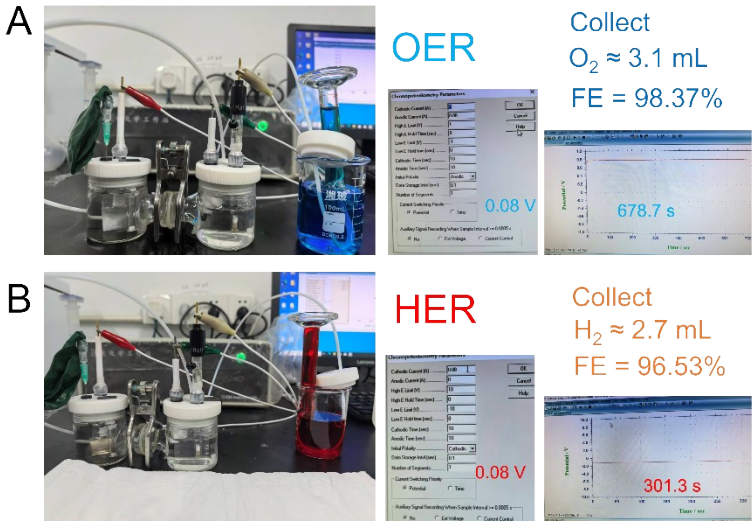


**Figure S17.** The $O_2$ (A) and $H_2$ (B) were collected by the water displacement method.

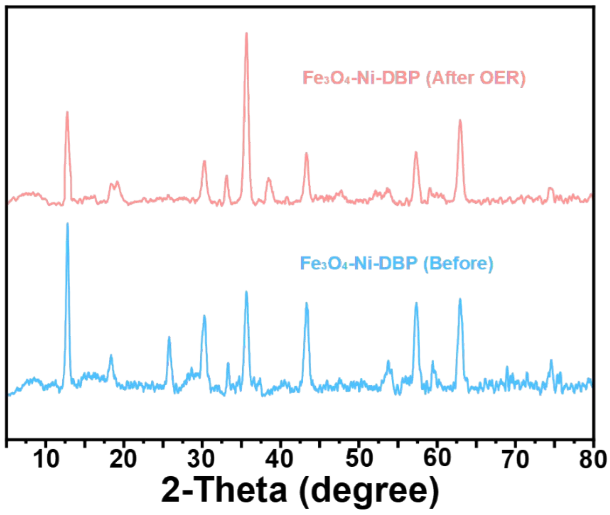


**Figure S18.** PXRD patterns of $Fe_3O_4$-Ni-DBP before and after OER in 1.0 M KOH.

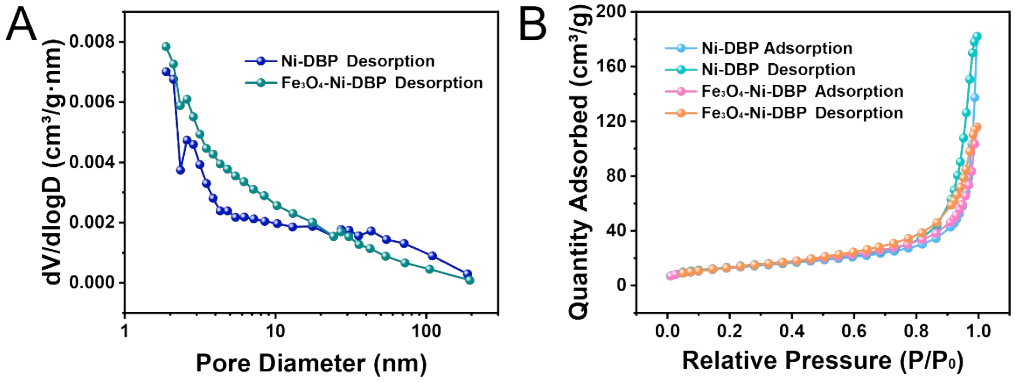


**Figure S19.** (A) $N_2$ adsorption-desorption isotherms and (B) cumulative pore-diameter distribution of pristine Ni-DBP/NF and $Fe_3O_4$-Ni-DBP/NF catalyst after long-term redox cycling.

**Table S3** BET surface area, pore volume and average pore diameter of Ni-DBP/NF and $Fe_3O_4$-Ni-DBP/NF.

| Samples | $S_{BET}$ ($m^2/g$) | Pore volume ($cm^3/g$) | Average pore diameter (nm) |
|---|---|---|---|
| Ni-DBP | 47.45 | 0.28 | 23.74 |
| $Fe_3O_4$-Ni-DBP | 49.49 | 0.18 | 13.70 |

## Reference


1 Shaddad, M. N.; Alharthi, A. I.; Aladeemy, S. A.;Arunachalam, P., Engineering oxygen vacancy on nickel-doped iron oxide nanorods as efficient bifunctional electrocatalysts for oxygen evolution and urea oxidation reaction. *J. Taiwan Inst. Chem. E.* **2025,** *177*, 105928.

2 Wei, X.; Wang, Y.; Wang, Y.; Chai, Y.;Liu, N., Improved OER electrocatalytic performance of Co-MOF by forming heterojunction with lower-conductivity $WO_3$ nanorods or $Cr_2O_3$ nanoparticles. *Int. J. Hydrogen Energ.* **2024,** *58*, 1240-1248.

3 Wu, F.; Jiao, Y.; Ge, J.; Feng, C.; Wu, Z.; Zhu, Y.;Li, Q., Formation of Ni-MOF derived nickel sulfides as efficient electrocatalysts for oxygen evolution reaction through optimizing the sulfur sources selection. *ChemistrySelect* **2024,** *9* (37), e202403487.

4 Ji, L.; Wei, Y.; Wu, P.; Xu, M.; Wang, T.; Wang, S.; Liang, Q.; Meyer, T. J.;Chen, Z., Heterointerface engineering of $Ni_2P$-$Co_2P$ nanoframes for efficient water splitting. *Chem. Mater.* **2021,** *33* (23), 9165-9173.

5 Hu, J.; Zhu, S.; Liang, Y.; Wu, S.; Li, Z.; Luo, S.;Cui, Z., Self-supported $Ni_3Se_2$@NiFe layered double hydroxide bifunctional electrocatalyst for overall water splitting. *J. Colloid. Interf. Sci.* **2021,** *587*, 79-89.

6 Huang, J.; Wang, S.; Nie, J.; Huang, C.; Zhang, X.; Wang, B.; Tang, J.; Du, C.; Liu, Z.;Chen, J., Active site and intermediate modulation of 3D $CoSe_2$ nanosheet array on Ni foam by Mo doping for high-efficiency overall water splitting in alkaline media. *Chem. Eng. J.* **2021,** *417*, 128055.

7 Yin, Z.; Liu, X.; Chen, S.; Xie, H.; Gao, L.; Liu, A.; Ma, T.;Li, Y., Interface engineering of the $MoS_2$/$NiS_2$/$CoS_2$ nanotube as a highly efficient bifunctional electrocatalyst for overall water splitting. *Mater. Today Nano* **2022,** *17*, 100156.

8 Goswami, A.; Ghosh, D.; Pradhan, D.; Biradha, K., In situ grown Mn(II) MOF upon nickel foam acts as a robust self-supporting bifunctional electrode for overall water splitting: A bimetallic synergistic collaboration strategy. *ACS Appl. Mater. Interfaces* **2022,** *14* (26), 29722-29734.

9 Li, C.; Zhang, Z.;Liu, R., In situ growth of 3D NiFe LDH-POM micro-flowers on nickel foam for overall water splitting. *Small* **2020,** *16* (46), 2003777.

10 Gong, Z.; Dai, Z.; Dong, Z.; Liu, Q.; Milichko, V. A.; Liu, H.; Liu, J.; Niu, R.;Gong, J., Green synthesis of luminescent La-MOF nanoparticle from waste poly(ethylene terephthalate) for high-

performance in Fe(III) detection. *Rare Met.* **2024,** *43* (8), 3833-3843.